J. Fluid Mech. (2014), *vol.* 755, R7, doi:10.1017/jfm.2014.459

JFM RAPIDS
journals.cambridge.org/rapids

The wave-induced added mass of walking droplets

John W. M. Bush[1,†], **Anand U. Oza**[1] **and Jan Moláček**[2]

[1]Department of Mathematics, Massachusetts Institute of Technology, Cambridge, MA 02139, USA

[2]Max Planck Institute for Dynamics and Self-Organization, 37077 Göttingen, Germany

(Received 9 May 2014; revised 21 July 2014; accepted 5 August 2014)

It has recently been demonstrated that droplets walking on a vibrating fluid bath exhibit several features previously thought to be peculiar to the microscopic realm. The walker, consisting of a droplet plus its guiding wavefield, is a spatially extended object. We here examine the dependence of the walker mass and momentum on its velocity. Doing so indicates that, when the walker's time scale of acceleration is long relative to the wave decay time, its dynamics may be described in terms of the mechanics of a particle with a speed-dependent mass and a nonlinear drag force that drives it towards a fixed speed. Drawing an analogy with relativistic mechanics, we define a hydrodynamic boost factor for the walkers. This perspective provides a new rationale for the anomalous orbital radii reported in recent studies.

Key words: drops, Faraday waves, waves/free-surface flows

1. Introduction

The first analogues of single-particle quantum systems emerged in the last decade from the laboratory of Yves Couder. Protière, Boudaoud & Couder (2006) demonstrated that millimetric drops on the surface of a vibrating bath may interact with their own wavefield in such a way as to walk steadily across the bath (Couder *et al.* 2005). These 'walkers' are spatially extended objects comprising both a particle and a wave. By virtue of their spatial delocalization, the walkers exhibit several features previously thought to be peculiar to the microscopic realm, including single-particle diffraction and interference (Couder & Fort 2006), tunnelling (Eddi *et al.* 2009), quantized orbits (Fort *et al.* 2010; Harris & Bush 2014; Oza *et al.* 2014; Perrard *et al.* 2014*a*,*b*) and orbital level splitting in a rotating frame (Eddi *et al.* 2012; Oza *et al.* 2014), and wave-like statistics in confined geometries (Harris *et al.* 2013). The relationship between this hydrodynamic system and various realist models of quantum dynamics is discussed by Bush (2015).

† Email address for correspondence: bush@math.mit.edu

Einstein (Bohm & Hiley 1982) and de Broglie (de Broglie 1926, 1987) both sought to reconcile quantum mechanics and relativity through consideration of the wave nature of matter (Chebotarev 2000). De Broglie's conception in his double-solution theory (de Broglie 1956) was of microscopic particles moving in resonance with and being guided by their own wavefield. While neither the physical origin nor the detailed geometric form of the pilot wavefield was specified, it was posited that the resulting particle motion could give rise to a statistical behaviour consistent with the predictions of standard quantum theory. Workers in stochastic electrodynamics (de la Peña & Cetto 1996) have suggested that an electromagnetic pilot wave might arise through the resonant interaction between a microscopic particle's internal vibration and the electromagnetic vacuum field (Boyer 2011). Some have further proposed that the interaction of moving particles with this vacuum field could give rise to a speed-dependent inertial mass, a feature of relativistic mechanics (Haisch & Rueda 2000; Rueda & Haisch 2005). We here explore the relevance of this perspective to the dynamics of walking droplets by inferring their wave-induced added mass.

By considering the detailed dynamics of droplet impact, Moláček & Bush (2013*a*,*b*) developed a theoretical model of droplets bouncing on a vibrating fluid bath that rationalizes all reported bouncing and walking behaviours (Wind-Willassen *et al.* 2013). By considering the destabilizing influence of the droplet's wavefield on its stationary bouncing, Moláček & Bush (2013*b*) rationalized the transition from bouncing to walking, and the limited extent of the walking regime. By averaging the forces acting on the droplet over the bouncing period, they developed a trajectory equation to describe the horizontal motion of the walkers. This trajectory equation was transformed into an integro-differential form by Oza, Rosales & Bush (2013), who treated the drop as a continuous rather than a discrete source of waves. Their model adequately rationalized the observed dependence of the walker speed on the system parameters and the stability of the walking states. Moreover, it has been successfully benchmarked through a combined experimental (Harris & Bush 2014) and theoretical (Oza *et al.* 2014) investigation of walkers in a rotating frame, yielding a new rationale for the emergence of quantized orbits (Fort *et al.* 2010) and wave-like statistics (Harris & Bush 2014). Their trajectory equation represents the starting point of the current study.

The hydrodynamic pilot-wave system is forced and dissipative. Nevertheless, it is interesting to imagine how the system might be described if one were unaware that it was either. Specifically, if one observes the system from above, and ignores the fact that it is a forced dissipative pilot-wave system, how should one describe the dynamics? What is the effective mass of a walker? We demonstrate here that, in the weak-acceleration limit, the walker dynamics may be described in terms of the motion of a particle with a speed-dependent mass and a nonlinear drag force that drives it towards a fixed speed.

2. Pilot-wave hydrodynamics

We consider a fluid bath with kinematic viscosity ν, density ρ, surface tension σ and depth H vibrating vertically with amplitude A_0, frequency $f = \omega/2\pi$ and acceleration $\gamma \cos \omega t$. When the acceleration amplitude $\gamma = A_0\omega^2$ exceeds a critical value corresponding to the Faraday threshold γ_F, the interface becomes unstable to a field of Faraday waves with frequency $\omega_F = \omega/2$, period $T_F = 2\pi/\omega_F$ and wavelength $\lambda_F = 2\pi/k_F$ prescribed by the standard water-wave dispersion relation, $\omega_F^2 = (gk_F + \sigma k_F^3/\rho)\tanh k_F H$ (Faraday 1831; Benjamin & Ursell 1954). The physical

system of interest arises when a millimetric droplet is placed on the surface of the vibrating bath when $\gamma < \gamma_F$. The interface would thus remain flat were it not for the drop impact.

2.1. *The trajectory equation*

In a parameter regime described by Protière *et al.* (2005, 2006) and Eddi *et al.* (2008) and rationalized by Moláček & Bush (2013*a*,*b*) and Wind-Willassen *et al.* (2013), a droplet of undeformed radius R placed on a vibrating bath may bounce indefinitely on the free surface in a variety of bouncing states (Wind-Willassen *et al.* 2013). Once the amplitude of the drop has increased sufficiently that the bouncing period is commensurate with that of the subharmonic Faraday waves generated locally by the drop impact, the bouncing state may be destabilized into a walking state (Protière *et al.* 2006). When γ exceeds the walking threshold γ_W, the droplet thus self-propels through resonant interaction with its own wavefield. The propulsive force arises as a result of the droplet landing on the sloping crest of its wavefield: with each impact, the bath exerts a horizontal impulse to the droplet. Moláček & Bush (2013*a*,*b*) developed a detailed description of the physics of impact, demonstrating that, in the parameter regime of interest, the interface behaves like a logarithmic spring, applying a force to the droplet that increases logarithmically with depth of penetration. They thus derived a trajectory equation for the resulting walking motion, time-averaging of which yields a description of the droplet's horizontal motion:

$$m\ddot{\boldsymbol{x}} + D\dot{\boldsymbol{x}} = -mg\nabla h(\boldsymbol{x}, t) + \boldsymbol{F}, \tag{2.1}$$

where $\boldsymbol{F}$ is an arbitrary applied body force, and the drag coefficient resulting from the walker's free flight and impact may be expressed as

$$D = Cmg\sqrt{\frac{\rho R}{\sigma}} + 6\pi\mu_a R\left(1 + \frac{\pi\rho_a g R}{6\mu_a\omega}\right), \tag{2.2}$$

where μ_a and ρ_a are the dynamic viscosity and density of air, and $C = 0.17$ was inferred from the coefficient of tangential restitution in the small-drop parameter regime of interest. Moláček & Bush (2013*b*) demonstrated that the wavefield resulting from the droplet's previous impacts may be approximated by

$$h(\boldsymbol{x}, t) = \sum_{n=-\infty}^{\lfloor t/T_F\rfloor} AJ_0(k_F|\boldsymbol{x} - \boldsymbol{x}_p(nT_F)|)\mathrm{e}^{-(t-nT_F)/T_M}. \tag{2.3}$$

For $\nu = 20$ cS and $f = 80$ Hz, the wave amplitude A and memory time T_M are given by

$$A = \frac{1}{2}\sqrt{\frac{\nu}{T_F}}\frac{k_F^3}{3k_F^2\sigma + \rho g}mgT_F\sin\Phi \quad \text{and} \quad T_M(\gamma) = \frac{T_d}{(1 - \gamma/\gamma_F)}, \tag{2.4}$$

where Φ is the mean phase of the wave during the contact time and $T_d \approx 0.0182$ s is the decay time of the waves in the absence of forcing (Moláček & Bush 2013*b*). Provided that the time scale of horizontal motion, $T_H = \lambda_F/|\dot{\boldsymbol{x}}_p|$, is much greater than that of vertical motion, T_F, as is the case for walkers, we may replace the summation

by the integral

$$h(\boldsymbol{x}, t) = \frac{A}{T_F} \int_{-\infty}^{t} J_0(k_F|\boldsymbol{x} - \boldsymbol{x}_p(s)|) \mathrm{e}^{-(t-s)/T_M} \, \mathrm{d}s. \tag{2.5}$$

The trajectory equation (2.1) thus takes an integro-differential form:

$$m\ddot{\boldsymbol{x}} + D\dot{\boldsymbol{x}} = \frac{W}{T_F} \int_{-\infty}^{t} J_1\left(k_F|\boldsymbol{x}(t) - \boldsymbol{x}(s)|\right) \frac{\boldsymbol{x}(t) - \boldsymbol{x}(s)}{|\boldsymbol{x}(t) - \boldsymbol{x}(s)|} \mathrm{e}^{-(t-s)/T_M} \mathrm{d}s + \boldsymbol{F}, \tag{2.6}$$

where $W = mgAk_F$ (Oza *et al.* 2013). Introducing the dimensionless variables $\hat{\boldsymbol{x}} = k_F\boldsymbol{x}$ and $\hat{t} = t/T_M$, we obtain

$$\kappa\hat{\boldsymbol{x}}'' + \hat{\boldsymbol{x}}' = \beta \int_0^{\infty} J_1\left(\left|\hat{\boldsymbol{x}}(\hat{t}) - \hat{\boldsymbol{x}}(\hat{t} - z)\right|\right) \frac{\hat{\boldsymbol{x}}(\hat{t}) - \hat{\boldsymbol{x}}(\hat{t} - z)}{\left|\hat{\boldsymbol{x}}(\hat{t}) - \hat{\boldsymbol{x}}(\hat{t} - z)\right|} \mathrm{e}^{-z} \, \mathrm{d}z + \hat{\boldsymbol{F}}, \tag{2.7}$$

where $\kappa = m/DT_M$ and $\beta = Wk_FT_M^2/DT_F$ are the non-dimensional mass and the memory force coefficient, $\hat{\boldsymbol{F}} = \boldsymbol{F}k_FT_M/D$ is the dimensionless applied force, and primes denote differentiation with respect to $\hat{t}$.

2.2. *The weak-acceleration limit*

We now consider the simplified dynamics that arises when the walker accelerates in response to a force that varies slowly relative to the memory time T_M, that is, $\hat{\boldsymbol{F}} = \hat{\boldsymbol{F}}(\epsilon t/T_M)$, where $0 < \epsilon \ll 1$. In this weak-acceleration limit, the walker velocity varies slowly relative to the time scale T_M, so we may write $\hat{\boldsymbol{x}}' = \boldsymbol{v}(\epsilon t/T_M)$.

We proceed by expanding the integral (2.7) in powers of ϵ. Since

$$\hat{\boldsymbol{x}}(\hat{t}) - \hat{\boldsymbol{x}}(\hat{t} - z) = \boldsymbol{v}(\epsilon\hat{t})z - \frac{\epsilon}{2}\boldsymbol{v}'(\epsilon\hat{t})z^2 + O(\epsilon^2), \tag{2.8}$$

we obtain

$$\begin{aligned} &J_1\left(\left|\hat{\boldsymbol{x}}(\hat{t}) - \hat{\boldsymbol{x}}(\hat{t} - z)\right|\right) \frac{\hat{\boldsymbol{x}}(\hat{t}) - \hat{\boldsymbol{x}}(\hat{t} - z)}{\left|\hat{\boldsymbol{x}}(\hat{t}) - \hat{\boldsymbol{x}}(\hat{t} - z)\right|} \\ &\quad = \frac{\boldsymbol{v}}{|\boldsymbol{v}|} J_1\left(|\boldsymbol{v}|\, z\right) + \frac{\epsilon}{2\,|\boldsymbol{v}|} \left\{ \left[\frac{\boldsymbol{v}\,(\boldsymbol{v}\cdot\boldsymbol{v}')}{|\boldsymbol{v}|^2} - \boldsymbol{v}' \right] J_1\left(|\boldsymbol{v}|\, z\right) z \right. \\ &\qquad \left. - \frac{\boldsymbol{v}\,(\boldsymbol{v}\cdot\boldsymbol{v}')}{|\boldsymbol{v}|} J_1'\left(|\boldsymbol{v}|\, z\right) z^2 \right\} + O(\epsilon^2), \end{aligned} \tag{2.9}$$

which yields

$$\begin{aligned} &\int_0^{\infty} J_1\left(\left|\hat{\boldsymbol{x}}(\hat{t}) - \hat{\boldsymbol{x}}(\hat{t} - z)\right|\right) \frac{\hat{\boldsymbol{x}}(\hat{t}) - \hat{\boldsymbol{x}}(\hat{t} - z)}{\left|\hat{\boldsymbol{x}}(\hat{t}) - \hat{\boldsymbol{x}}(\hat{t} - z)\right|} \mathrm{e}^{-z} \, \mathrm{d}z \\ &\quad = \frac{\boldsymbol{v}}{|\boldsymbol{v}|^2} \left(1 - \frac{1}{\sqrt{1 + |\boldsymbol{v}|^2}} \right) + \frac{\epsilon}{2\,|\boldsymbol{v}|} \left\{ \left[\frac{\boldsymbol{v}\,(\boldsymbol{v}\cdot\boldsymbol{v}')}{|\boldsymbol{v}|^2} - \boldsymbol{v}' \right] \frac{\boldsymbol{v}}{\left(1 + |\boldsymbol{v}|^2\right)^{3/2}} \right. \\ &\qquad \left. - \frac{\boldsymbol{v}\,(\boldsymbol{v}\cdot\boldsymbol{v}')}{|\boldsymbol{v}|} \frac{1 - 2\,|\boldsymbol{v}|^2}{\left(1 + |\boldsymbol{v}|^2\right)^{5/2}} \right\} + O(\epsilon^2). \end{aligned} \tag{2.10}$$

The trajectory equation (2.7) thus takes the form

$$\kappa\hat{\boldsymbol{x}}''+\hat{\boldsymbol{x}}'=\frac{\beta\hat{\boldsymbol{x}}'}{\left|\hat{\boldsymbol{x}}'\right|^2}\left(1-\frac{1}{\sqrt{1+\left|\hat{\boldsymbol{x}}'\right|^2}}\right)+\frac{\beta}{2}\left[\frac{3\left(\hat{\boldsymbol{x}}'\cdot\hat{\boldsymbol{x}}''\right)\hat{\boldsymbol{x}}'}{\left(1+\left|\hat{\boldsymbol{x}}'\right|^2\right)^{5/2}}-\frac{\hat{\boldsymbol{x}}''}{\left(1+\left|\hat{\boldsymbol{x}}'\right|^2\right)^{3/2}}\right]+\hat{\boldsymbol{F}}+O(\epsilon^2), \tag{2.11}$$

which may be expressed as

$$\frac{\mathrm{d}}{\mathrm{d}\hat{t}}\left(\kappa\gamma_B\hat{\boldsymbol{x}}'\right)+\hat{\boldsymbol{x}}'\left[1-\frac{\beta}{\left|\hat{\boldsymbol{x}}'\right|^2}\left(1-\frac{1}{\sqrt{1+\left|\hat{\boldsymbol{x}}'\right|^2}}\right)\right]=\hat{\boldsymbol{F}}+O(\epsilon^2), \tag{2.12}$$

where the hydrodynamic boost factor is defined as

$$\gamma_B=\gamma_B\left(\left|\boldsymbol{x}'\right|\right)=1+\frac{\beta}{2\kappa\left(1+\left|\hat{\boldsymbol{x}}'\right|^2\right)^{3/2}}. \tag{2.13}$$

We note that, in the absence of an applied force ($\hat{\boldsymbol{F}}=0$), (2.12) has a solution

$$\left|\hat{\boldsymbol{x}}'\right|=\hat{u}_0\equiv\frac{1}{\sqrt{2}}\left(-1+2\beta-\sqrt{1+4\beta}\right)^{1/2}. \tag{2.14}$$

This corresponds precisely to the formula for the free rectilinear walking speed of a droplet, which was found to adequately rationalize the observed dependence of u_0 on the forcing acceleration γ (Oza *et al.* 2013).

In terms of dimensional variables, we may write the trajectory equation (2.12) as

$$\frac{\mathrm{d}}{\mathrm{d}t}\left(m\gamma_B\dot{\boldsymbol{x}}\right)+D_w\dot{\boldsymbol{x}}=\boldsymbol{F}, \tag{2.15}$$

where

$$D_w=D_w(|\dot{\boldsymbol{x}}|)=D\left[1-\frac{mgA}{DT_F\left|\dot{\boldsymbol{x}}\right|^2}\left(1-\frac{1}{\sqrt{1+\left(k_FT_M\left|\dot{\boldsymbol{x}}\right|\right)^2}}\right)\right] \tag{2.16}$$

and

$$\gamma_B=1+\frac{gAk_F^2T_M^3}{2T_F\left(1+\left(k_FT_M\left|\dot{\boldsymbol{x}}\right|\right)^2\right)^{3/2}}. \tag{2.17}$$

We may rewrite the trajectory equation (2.15) in the form

$$\frac{\mathrm{d}\boldsymbol{p}_w}{\mathrm{d}t}+D_w\dot{\boldsymbol{x}}=\boldsymbol{F}, \tag{2.18}$$

so both the mass m_w and momentum $\boldsymbol{p}_w$ of the walker may now be expressed in terms of the hydrodynamic boost factor; specifically

$$\boldsymbol{p}_w=m_w\dot{\boldsymbol{x}},\quad\text{where } m_w=m\gamma_B. \tag{2.19}$$

In the weak-acceleration limit under consideration, the effect of the wave force on the walker dynamics is twofold. First, it augments the walker's effective mass by a factor γ_B that depends on its speed $|\dot{\boldsymbol{x}}|$. The dependence of γ_B on the walker speed u_0 and the forcing acceleration γ/γ_F is illustrated in figure 1. We note that γ_B decreases monotonically with speed through the entire walking regime, for $\gamma_w<\gamma<\gamma_F$. Second,

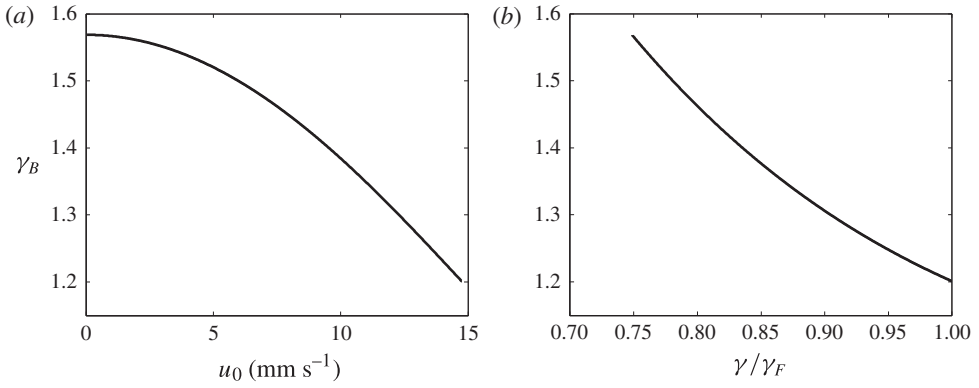

FIGURE 1. Dependence of the hydrodynamic boost factor γ_B on the walker speed $|\dot{\boldsymbol{x}}| = u_0(\gamma)$ and forcing acceleration γ/γ_F, for a walker of radius $R = 0.4$ mm and impact phase $\sin\Phi = 0.25$.

it generates a nonlinear drag coefficient D_w, where $D_w > 0$ if $|\dot{\boldsymbol{x}}| > u_0$ and $D_w < 0$ otherwise. The wave-induced drag thus acts as a restoring force that drives the walker towards its free walking speed u_0.

3. Response to a weak unidirectional force

We first consider the special case in which the slowly varying applied force is also weak and unidirectional. Specifically, we assume that the applied force is small relative to the drag, so that $|\boldsymbol{F}|k_F T_M/D = O(\epsilon)$. We thus write $\hat{\boldsymbol{F}} = \epsilon\hat{f}(\epsilon t/T_M)\boldsymbol{s}$, where $\boldsymbol{s}$ is a constant unit vector.

For the remainder of this section, we assume all variables to be dimensionless and drop all hats. In the Cartesian coordinate system in which $\boldsymbol{s} = [1, 0]$, we write $\dot{\boldsymbol{x}} = v(T)\,[\cos\theta(T), \sin\theta(T)]$, where $T = \epsilon t$. The equations of motion (2.12) take the form

$$m_w(v)v\theta' = -f(T)\sin\theta + O(\epsilon), \tag{3.1}$$

$$\epsilon\frac{\mathrm{d}}{\mathrm{d}T}\left(m_w(v)v\right) + D_w(v)v = \epsilon f(T)\cos\theta + O(\epsilon^2), \tag{3.2}$$

where

$$m_w(v) = \kappa\gamma_B(v) \quad \text{and} \quad D_w(v) = 1 - \frac{\beta}{v^2}\left(1 - \frac{1}{\sqrt{1+v^2}}\right) \tag{3.3}$$

are the dimensionless wave-induced mass and drag, as introduced in § 2.2, and primes denote differentiation with respect to the slow time scale T.

To leading order in ϵ, the walker will move at its free walking speed u_0. To examine the perturbation from the steady walking solution, we substitute $v = u_0 + \epsilon u_1(T)$ into (3.1)–(3.2) and deduce

$$m_w(u_0)u_0\theta' = -f\sin\theta + O(\epsilon), \quad \tilde{D}_w(u_0)u_1 = f\cos\theta + O(\epsilon), \tag{3.4}$$

where

$$\tilde{D}_w(u_0) = \frac{\mathrm{d}}{\mathrm{d}v}\left(D_w(v)v\right)\bigg|_{v=u_0}. \tag{3.5}$$

Equations (3.4) may be readily solved to obtain

$$\left|\tan\frac{\theta(T)}{2}\right| = \left|\tan\frac{\theta(0)}{2}\right| \exp\left(-\frac{F(T)}{m_w(u_0)u_0}\right), \quad v(T) = u_0 + \frac{\epsilon f(T)\cos\theta(T)}{\tilde{D}_w(u_0)} + O(\epsilon^2), \tag{3.6}$$

where $F'(T) = f(T)$ and $F(0) = 0$. These expressions uniquely determine the evolution of the walking speed $v(T)$ and direction $\theta(T)$. When the applied force f is constant, the solution (3.6) implies that the walker's direction θ approaches that of the force over the time scale $T_\theta = m_w(u_0)u_0/|f|$. Thus, the turning time scale T_θ is prescribed by the ratio of the walker's modified momentum $p_w(u_0)$ to the applied force, and is independent of the drag.

4. Orbital motion

We now consider the case of circular motion of the form $\boldsymbol{x}(t) = (r_0\cos\omega t, r_0\sin\omega t)$. Defining $\boldsymbol{t} = (-\sin\omega t, \cos\omega t)$ and $\boldsymbol{n} = (\cos\omega t, \sin\omega t)$ as the unit tangent and outward normal vectors, respectively, allows us to write the normal and tangential components of (2.15) in the form

$$-m\gamma_B r_0\omega^2 = \boldsymbol{F}\cdot\boldsymbol{n}, \tag{4.1}$$

$$r_0\omega\left[D - \frac{mgA}{T_F(r_0\omega)^2}\left(1 - \frac{1}{\sqrt{1+(k_F T_M r_0\omega)^2}}\right)\right] = \boldsymbol{F}\cdot\boldsymbol{t}, \tag{4.2}$$

where γ_B is defined in (2.17) with $|\dot{\boldsymbol{x}}| = r_0\omega$. The weak-acceleration approximation of § 2.2 holds provided that the velocity $\dot{\boldsymbol{x}}$ varies slowly relative to the memory time, or, equivalently, the orbital period is much larger than the decay time of the wavefield, $T_M \ll T_{orb} \equiv 2\pi r_0/u_0$. In this case, the walker does not interact with its own wake, specifically, the wavefield generated by its previous orbit. This limit thus corresponds to the weak-orbital-memory limit defined in Oza *et al.* (2014), in which orbital quantization does not arise. We consider in turn inertial orbits arising in a rotating frame, and circular orbits arising in the presence of a central force arising from a harmonic potential.

4.1. *Walking in a rotating frame*

When an object of mass m translates in a horizontal plane at a constant speed u in a frame rotating about a vertical axis with constant angular speed Ω, it will in general move along a circular orbit. The radius R_c and frequency $\omega_c = -u/R_c$ of such an inertial orbit are prescribed by the balance between the outwards inertial force, mu^2/R_c, and the inwards Coriolis force, $2mu\Omega$; thus, $R_c = u/2\Omega$ and $\omega_c = -2\Omega$. In their examination of droplets walking in a rotating frame, Fort *et al.* (2010) demonstrated that at high memory, the influence of the wave force leads to orbital quantization on the Faraday wavelength, and that such quantized orbits are analogous to the Landau levels that arise for electric charges moving in the presence of a uniform magnetic field. In the low-memory limit, they report that the inertial orbits vary continuously with rotation rate, but that the orbits are typically 20–50 % larger than would be expected from the classical balance. This orbital offset, as further detailed in Harris & Bush (2014) and Oza *et al.* (2014), may be readily understood on the basis of the foregoing developments.

For circular motion in the presence of a Coriolis force $\boldsymbol{F} = -2m\boldsymbol{\Omega}\times\dot{\boldsymbol{x}}$, the tangential component of the force vanishes, $\boldsymbol{F}\cdot\boldsymbol{t} = 0$, so the tangential force balance

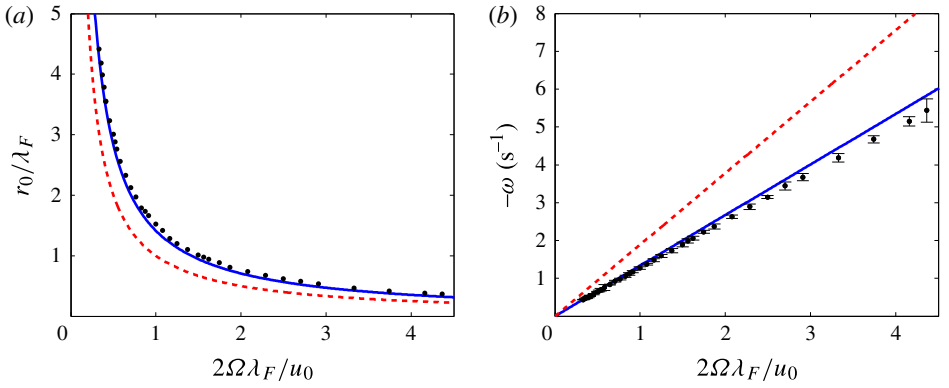

FIGURE 2. The observed dependence of the orbital radius r_0 and frequency ω on the rotation rate Ω for a droplet walking at speed u_0 in a rotating frame in the low-memory regime ($\nu = 20.9$ cS, $T_d = 0.0174$ s, $R = 0.40$ mm, $u_0 = 9.0$ mm s^{-1}, $\gamma/\gamma_F = 0.82$, $\sin\Phi = 0.26$). The experimental data are those reported by Harris & Bush (2014), and the value of $\sin\Phi$ is chosen to match the experimentally observed free walking speed u_0. The dashed lines indicate the standard solutions for inertial orbits, $r_0 = R_c \equiv u_0/2\Omega$ and $\omega = \omega_c \equiv -2\Omega$. The solid lines correspond to the predictions of (4.3), which incorporate the walker's hydrodynamic boost factor, $\gamma_B = 1.41$.

(4.2) requires that the orbital speed correspond to the free walking speed $u_0 \equiv r_0|\omega|$. The radial force balance (4.1) then indicates the dependence of the orbital frequency and radius on the boost factor,

$$\omega = -\frac{2\Omega}{\gamma_B}, \qquad r_0 = \gamma_B \frac{u_0}{2\Omega}. \tag{4.3}$$

The net effect of the wavefield is thus to decrease the orbital frequency and increase the orbital radius relative to the standard results, ω_c and R_c. Figure 2 indicates the observed dependence of the orbital radius and orbital frequency on the rotation rate at low memory reported by Harris & Bush (2014). The dashed lines indicate the standard results, $R_c = u_0/2\Omega$ and $\omega_c = -2\Omega$, while the solid lines correspond to our predictions (4.3), which incorporate the boost factor.

4.2. *Walking in a central force*

Perrard *et al.* (2014*b*) report the results of a study of walker motion in the presence of a central force. By encapsulating ferrofluid within a walker, and applying a vertical magnetic field with a radial gradient, they produced a force field that increased linearly with radius, $\boldsymbol{F} = -k\boldsymbol{x}$. In certain regimes, orbital motions were observed; in others, more complex periodic and aperiodic motions arose. We focus here on the circular orbits reported. From the classical balance of the applied force kR and inertial force mu_0^2/R, one expects circular orbits with radius $R_h = u_0\sqrt{m/k}$ and frequency $\omega_h = \sqrt{k/m}$. Like their counterparts arising in the rotating frame, the observed orbits exhibited a radial offset, being typically 10 % larger than R_c, an observation we can now rationalize.

For circular motion in the presence of a central force $\boldsymbol{F} = -k\boldsymbol{x}$, once again $\boldsymbol{F}\cdot\boldsymbol{t} = 0$, so the tangential force balance (4.2) requires that the orbital speed correspond to

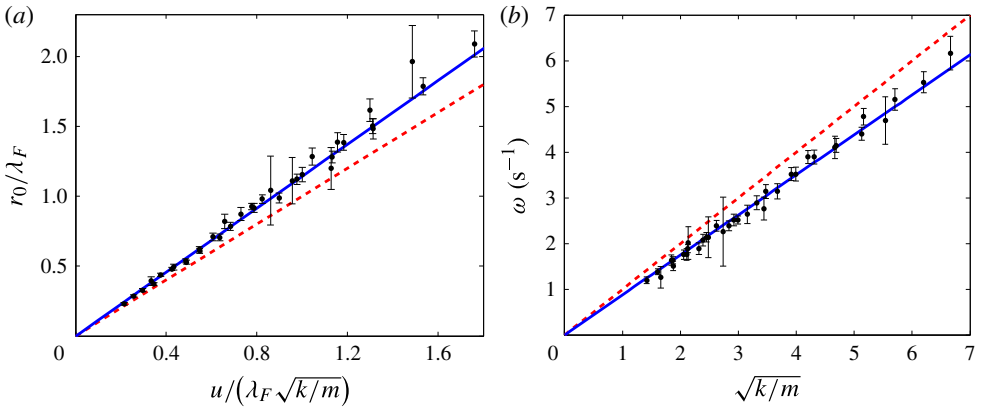

FIGURE 3. The observed dependence of the orbital radius r_0 and frequency ω on the spring constant k for a droplet walking at speed u_0 under a spring force $\boldsymbol{F} = -k\boldsymbol{x}$ in the low-memory regime. The experimental parameters were reported to be $\nu = 20$ cS, $T_d = 0.0182$ s, $R = 0.40$ mm, $u_0 = 12.2$ mm s^{-1}, $\gamma/\gamma_F = 0.9$ and $\sin\Phi = 0.25$ (Perrard & Couder, private communication). The value of the phase $\sin\Phi$ is chosen to match the experimentally observed free walking speed u_0. The dashed lines indicate the standard solutions, $r_0 = R_h \equiv u_0/\sqrt{k/m}$ and $\omega = \omega_h \equiv \sqrt{k/m}$. The solid lines correspond to the predictions of (4.4), which incorporate the walker's hydrodynamic boost factor, $\gamma_B = 1.30$.

the free walking speed $u_0 \equiv r_0|\omega|$. The radial force balance (4.1) then indicates the dependence of the orbital frequency and radius on the boost factor,

$$\omega = \sqrt{\frac{k}{m\gamma_B}}, \quad r_0 = \sqrt{\gamma_B}\frac{u_0}{\sqrt{k/m}}. \tag{4.4}$$

Once again, the net effect of the wavefield is thus to decrease the orbital frequency, and to increase the orbital radius relative to the standard results, ω_h and R_h. Figure 3 indicates the observed dependence of the orbital radius and orbital frequency on the spring constant at low memory reported by Perrard *et al.* (2014*b*). The dashed lines indicate the standard results, $R_h = u_0\sqrt{m/k}$ and $\omega_h = \sqrt{k/m}$, while the solid lines correspond to our predictions (4.4), which incorporate the boost factor.

For the case of orbital dynamics, one can rationalize the increase of the orbital radius relative to that expected in the absence of the wave force through consideration of the geometry of the pilot wavefield (Oza *et al.* 2014). In the low-memory limit, the drop is influenced primarily by the wave generated by its most recent impact. As the drop is turning in a circular orbit, the wave force generated during impact necessarily has a radial component, the result being an increase in the orbital radius.

We note that Labousse & Perrard (2014) proposed the following equation to describe the dynamics of a walker acted upon by a central force in the low-memory regime:

$$m\ddot{\boldsymbol{x}} + D_w\dot{\boldsymbol{x}} = -k\boldsymbol{x}, \quad D_w = D\left(\frac{|\dot{\boldsymbol{x}}|^2}{u_0^2} - 1\right). \tag{4.5}$$

This trajectory equation captures certain features of (2.15); in particular, the nonlinear drag coefficient D_w acts as a restoring force that drives the walker towards its free walking speed u_0. However, in neglecting the contribution of the walker's

wave-induced added mass, it cannot account for the anomalously large orbital radii reported in laboratory experiments and rationalized above.

5. Discussion

A droplet walking in resonance with its own monochromatic wavefield represents a rich dynamical system, the first realization of a double-wave pilot-wave system of the form envisaged by de Broglie (1926, 1956, 1987). While Couder and coworkers have highlighted the quantum mechanical aspects of walkers as they emerge in the high-path-memory limit (Couder & Fort 2006; Fort *et al.* 2010; Harris *et al.* 2013), we have here explored their first tentative connections to relativistic mechanics. The leading-order force balance on the walker is between a propulsive wave force and a viscous drag term. The steady walking state is sustained by vibrational forcing: the mechanical work done by the vibration balances the viscous dissipation. In the weak-acceleration limit, the walker's motion may be described in terms of the mechanics of a particle with a speed-dependent mass subject to a nonlinear restoring force that drives it towards a fixed speed. The relative magnitude of the effective mass of the walker and the droplet mass is prescribed by the hydrodynamic boost factor, whose dependence on the system parameters has been deduced. This boost factor is always greater than 1, and decreases with increasing speed in the weak-acceleration limit examined.

For the case of orbital dynamics, if the system were observed from above with no knowledge of either the vibrational forcing or the wavefield, the walker's motion might be described in terms of the inviscid dynamics of a particle whose mass depends on its speed. Doing so has allowed us to rationalize the offset in the radius of the walkers' inertial orbits in terms of their wave-induced added mass. Moreover, it has provided a more general framework for understanding and describing the walker dynamics.

Acknowledgements

The authors gratefully acknowledge the financial support of the NSF through Grants CBET-0966452 and CMMI-1333242, and that of the MIT-Brazil and CNPq-Science Without Borders programs. A.O. also acknowledges support from graduate fellowships through the NSF and Hertz Foundation. We thank S. Perrard, M. Labousse, E. Fort and Y. Couder for valuable discussions and the use of their data.

References

BENJAMIN, T. B. & URSELL, F. 1954 The stability of the plane free surface of a liquid in vertical periodic motion. *Proc. R. Soc. Lond.* A **225**, 505–515.

BOHM, D. J. & HILEY, B. J. 1982 The de Broglie pilot wave theory and the further development of new insights arising out of it. *Found. Phys.* **12** (10), 1001–1016.

BOYER, T. H. 2011 Any classical description of nature requires classical electromagnetic zero-point radiation. *Am. J. Phys.* **79**, 1163–1167.

DE BROGLIE, L. 1926 *Ondes et Mouvements*. Gauthier-Villars.

DE BROGLIE, L. 1956 *Une Tentative d'Interprétation Causale et Non Linéaire de la Mécanique Ondulatoire: la Théorie de la Double Solution*. Gauthier-Villars.

DE BROGLIE, L. 1987 Interpretation of quantum mechanics by the double solution theory. *Ann. Fond. Louis de Broglie* **12** (4), 1–23.

BUSH, J. W. M. 2015 Pilot-wave hydrodynamics. *Annu. Rev. Fluid Mech.* **47** (in press).

CHEBOTAREV, L. 2000 Introduction: the de Broglie–Bohm–Vigier approach in quantum mechanics. In *Jean-Pierre Vigier and the Stochastic Interpretation of Quantum Mechanics* (ed. S. Jeffers, B. Lehnert, N. Abramson & L. Chebotarev), Berkeley Press.

COUDER, Y. & FORT, E. 2006 Single-particle diffraction and interference at a macroscopic scale. *Phys. Rev. Lett.* **97**, 154101.

COUDER, Y., PROTIÈRE, S., FORT, E. & BOUDAOUD, A. 2005 Walking and orbiting droplets. *Nature* **437**, 208.

EDDI, A., FORT, E., MOISY, F. & COUDER, Y. 2009 Unpredictable tunneling of a classical wave–particle association. *Phys. Rev. Lett.* **102**, 240401.

EDDI, A., MOUKHTAR, J., PERRARD, S., FORT, E. & COUDER, Y. 2012 Level splitting at macroscopic scale. *Phys. Rev. Lett.* **108**, 264503.

EDDI, A., TERWAGNE, D., FORT, E. & COUDER, Y. 2008 Wave propelled ratchets and drifting rafts. *Europhys. Lett.* **82**, 44001.

FARADAY, M. 1831 On a peculiar class of acoustical figures, and on certain forms assumed by groups of particles upon vibrating elastic surfaces. *Phil. Trans. R. Soc. Lond.* **121**, 299–340.

FORT, E., EDDI, A., BOUDAOUD, A., MOUKHTAR, J. & COUDER, Y. 2010 Path-memory induced quantization of classical orbits. *Proc. Natl Acad. Sci.* **107** (41), 17515–17520.

HAISCH, B. & RUEDA, A. 2000 On the relation between a zero-point-field-induced inertial effect and the Einstein–de Broglie formula. *Phys. Rev.* A **268**, 421–427.

HARRIS, D. M. & BUSH, J. W. M. 2014 Droplets walking in a rotating frame: from quantized orbits to multimodal statistics. *J. Fluid Mech.* **739**, 444–464.

HARRIS, D. M., MOUKHTAR, J., FORT, E., COUDER, Y. & BUSH, J. W. M. 2013 Wavelike statistics from pilot-wave dynamics in a circular corral. *Phys. Rev.* E **88**, 011001.

LABOUSSE, M. & PERRARD, S. 2014 Non Hamiltonian features of a classical pilot-wave dynamics. *Phys. Rev.* E (in press).

MOLÁČEK, J. & BUSH, J. W. M. 2013*a* Drops bouncing on a vibrating bath. *J. Fluid Mech.* **727**, 582–611.

MOLÁČEK, J. & BUSH, J. W. M. 2013*b* Drops walking on a vibrating bath: towards a hydrodynamic pilot-wave theory. *J. Fluid Mech.* **727**, 612–647.

OZA, A. U., HARRIS, D. M., ROSALES, R. R. & BUSH, J. W. M. 2014 Pilot-wave dynamics in a rotating frame: on the emergence of orbital quantization. *J. Fluid Mech.* **744**, 404–429.

OZA, A. U., ROSALES, R. R. & BUSH, J. W. M. 2013 A trajectory equation for walking droplets: hydrodynamic pilot-wave theory. *J. Fluid Mech.* **737**, 552–570.

DE LA PEÑA, L. & CETTO, A. M. 1996 *The Quantum Dice: An Introduction to Stochastic Electrodynamics*. Kluwer Academic.

PERRARD, S., LABOUSSE, M., FORT, E. & COUDER, Y. 2014*a* Chaos driven by interfering memory. *Phys. Rev. Lett.* (in press).

PERRARD, S., LABOUSSE, M., MISKIN, M., FORT, E. & COUDER, Y. 2014*b* Self-organization into quantized eigenstates of a classical wave-driven particle. *Nat. Commun.* **5**, 3219.

PROTIÈRE, S., BOUDAOUD, A. & COUDER, Y. 2006 Particle–wave association on a fluid interface. *J. Fluid Mech.* **554**, 85–108.

PROTIÈRE, S., COUDER, Y., FORT, E. & BOUDAOUD, A. 2005 The self-organization of capillary wave sources. *J. Phys.: Condens. Matter* **17** (45), S3529–S3535.

RUEDA, A. & HAISCH, B. 2005 Gravity and the quantum vacuum inertia hypothesis. *Ann. Phys. (Leipzig)* **14** (8), 479–498.

WIND-WILLASSEN, Ø., MOLÁČEK, J., HARRIS, D. M. & BUSH, J. W. M. 2013 Exotic states of bouncing and walking droplets. *Phys. Fluids* **25**, 082002.